GDCh Research Article Angewandte International Edition Chemie www.angewandte.org

How to cite: *Angew. Chem. Int. Ed.* **2025**, *64*, e202505717
doi.org/10.1002/anie.202505717

Nanomotors **Hot Paper**

Fast and Autonomous Mannosylated Nanomotors for Dynamic Cancer Cell Targeting

Yuechi Liu, Roberto Terracciano, Jari Scheerstra, Gokhan Yilmaz, Hanglong Wu, Pascal Welzen, Shoupeng Cao, Tania Patino Padial, Loai Abdelmohsen, Jingxin Shao, Bingbing Sun,* C. Remzi Becer,* and Jan C. M. van Hest**

Abstract: An attractive strategy in cancer cell therapy is to employ motile nanoparticles that can actively search for their target. Herein, we introduce mannosylated compartmentalized cross-linked enzyme-driven nanomotors (c-CLEnM), which exhibit specific and efficient targeting of Hep G2 cells through elevated autonomous motion. In this design, we constructed biodegradable bowl-shaped stomatocytes encapsulating the enzymes glucose oxidase (GOx) and catalase (CAT) within their nanocavity. A subsequent enzyme crosslinking reaction was performed to guarantee their stability. Furthermore, the c-CLEnM were surface modified with a mannose-functional glycopolymer, enabling binding with receptors expressed on Hep G2 cells. Interestingly, the targeting ligands on the nanomotors not only improved their specificity toward cancer cells but also enhanced motility. Compared to the non-mannosylated nanomotors, mannosylated c-CLEnM exhibited enhanced motion and higher targeting efficiency to cells in glucose-containing ionic environments. The unexpected acceleration in speed resulted from the surface modification of these nanomotors with a glycopolymer layer, which increased the zeta potential and created a shielding effect that mitigated the influence of the surrounding ions. This nanomotor design highlights the synergistic effect of functional glycopolymer modification on cellular uptake, adding an additional level of control to nanomotors for application in cancer therapy.

Introduction

Autonomously powered nano- and micromotors are microscopic devices that convert various sources of energy into mechanical motion.[1–4] These nanomotors are classified based on the energy input they harness, including chemical propulsion mediated by enzymes and inorganic catalysts,[5] and activation by external fields such as light,[6] ultrasound,[7] and magnetism.[8] In contrast to typical passive cargo delivery systems, self-propelled nanomotors possess the capability to dynamically transport payloads to specific destinations. In this regard, enzyme-powered nanomotors have been often applied, as they can be driven by endogenous fuel sources. By exploiting higher fuel concentrations in target tissues, also efficiency and specificity of delivery can also be improved.[9–14] A further level of control can be achieved by decorating nanomotors with targeting ligands, such as antibodies[14] or aptamers.[15] This combined approach, however, has seen limited exploration to date. Furthermore, the effect of surface modification with targeting ligands on the motile features of the nanomotors has not been studied in detail yet.

An interesting class of targeting ligands are carbohydrates, such as mannose, which have proven to be particularly useful for cellular uptake through receptor-mediated internalization.[16] This efficacy is attributed to their strong affinity for receptors highly expressed on cancer cell membranes, such as lectins.[17] The effective binding furthermore does not impede endocytosis, which remains relatively unaffected by the size or composition of the glycan.[18] Additionally, carbohydrate-functionalized nanoparticles also allow multivalent ligand display for strong interaction with lectins.[19] This approach enhances the specificity and efficiency of cellular interactions, providing a promising avenue for the development of targeted drug delivery systems in cancer therapy. Recently, polysaccharide polymers have gained attention for their ability to target cancer cells.

[*] Y. Liu, J. Scheerstra, H. Wu, P. Welzen, T. P. Padial, L. Abdelmohsen, J. Shao, B. Sun, J. C. M. van Hest
Bio-Organic Chemistry, Institute of Complex Molecular Systems, Eindhoven University of Technology, Helix, P. O. Box 513, Eindhoven 5600 MB, the Netherlands
E-mail: J.Shao@tue.nl
b.sun@tue.nl
J.C.M.v.Hest@tue.nl

R. Terracciano, G. Yilmaz, C. R. Becer
Department of Chemistry, University of Warwick, Coventry CV4 7AL, UK
E-mail: Remzi.Becer@warwick.ac.uk

S. Cao
College of Polymer Science and Engineering, Sichuan University, Chengdu 610065, P.R. China

Additional supporting information can be found online in the Supporting Information section

Linear glycopolymers have multiple repeating units, which can provide numerous binding sites, offering benefits such as multivalency, customizability, reduced dosage and side effects, and improved cellular uptake by promoting prolonged contact with cell surfaces.[20,21] Moreover, linear glycopolymers are typically more stable and more effective than peptides and antibodies in biological medium.[16] Because of these benefits, they have been explored as targeting ligands in nanomedicine. Previously, we demonstrated how bowl-shaped stomatocytes can be created out of spherical polymersomes via an osmotically induced shape change process. Loading of the newly formed nanocavity with enzymes enabled the construction of nanomotors due to the intrinsic shape anisotropy of the stomatocytes.[22–24]

In this study, we aimed to construct stomatocyte nanomotors with targeting capacity. For this purpose, biodegradable poly(ethylene glycol)-*b*-poly(D,L-lactide) (PEG-PDLLA) stomatocytes were loaded with two enzymes, a well-known cascade developed in nanomotor-driven applications,[22,25] GOx and CAT, which were subsequently crosslinked to form compartmentalized cross-linked enzymatic nanomotors (c-CLEnM), which enables a cascade reaction to drive autonomous motion in the presence of the fuel glucose. Additionally, the surface of the particles was modified with a mannose-containing glycopolymer for specific targeting of cancer cells. We then investigated the targeting ability of these mannosylated nanomotors to receptors that are expressed on Hep G2 cells, possibly like the mannose receptor (MR).[26–29] The nanomotors showed effective accumulation on the Hep G2 cell membrane and elevated cellular uptake compared to galactosylated nanomotors, non-decorated nanomotors, and passive particles. Remarkably, not only was the targeting efficiency improved, but also the motility of the particles was enhanced significantly in cell culture environments. This unexpected acceleration in motility was a result of the surface modification of the nanomotors with the glycopolymer, which increased the zeta potential of particles, potentially generating a shielding effect that mitigates the influence of surrounding ions (Scheme 1).[30] This modification likely improved the ionic tolerance of the nanomotors, ultimately boosting their performance. Glycopolymer modification, therefore, led to a synergistic effect by improving both motility in a physiological environment and enabling targeting capability toward cancer cells. This study underscores the importance of understanding the effect of surface modification of nanomotors, as it could expand their potential applications in nanomedicine, offering a promising strategy to address the ion tolerance challenge in biological environments.

Results and Discussion

Construction of Compartmentalized Cross-Linked Enzymatic Nanomotor (c-CLEnM)

Biodegradable block copolymers, namely PEG_{44}-$PDLLA_{95}$, PEG_{22}-$PDLLA_{95,}$ and N_3-PEG_{67}-$PDLLA_{70}$, were synthesized through ring-opening polymerization (ROP), as detailed in previously published work.[23] The resulting block copolymers were analyzed via ^{1}H-nuclear magnetic resonance spectroscopy (NMR) and gel permeation chromatography (GPC) using DMF as eluent and PS standards. ^{1}H NMR measurements proved the formation of the targeted polymers (Figures S1–S3). GPC revealed molar mass dispersities ($Đ$) ranging between 1.08 and 1.20 (Figure S4). The formation of the compartmentalized cross-linked enzymatic nanomotor (c-CLEnM) occurred in four steps, as illustrated in Figure 1a. Initially, spherical polymersomes were self-assembled from block copolymers of PEG_{44}-$PDLLA_{95}$, PEG_{22}-$PDLLA_{95,}$ and N_3-PEG_{67}-$PDLLA_{70}$ 10:7:3 w/w/w through the traditional solvent switch methodology. Subsequently, the organic solvent was gradually removed via dialysis, inducing an osmotically driven shape transformation into stomatocytes. The formation of stomatocytes relied on the negative spontaneous curvature of the polymer membrane, which was attained via the blending of the block copolymers with different PEG lengths.[22,24] The distinct dual-compartmental structure of these azido stomatocytes was confirmed with scanning electron microscopy (SEM) (Figure 1b) and cryogenic transmission electron microscopy (cryo-TEM) (Figure 1c).

Following this, GOx and CAT were loaded into the lumen of stomatocytes during the shape change from polymersomes to stomatocytes. Subsequently, nonencapsulated enzymes were removed through spin filtration, followed by the concentration and dispersion of stomatocytes in MilliQ. The enzyme ratio within the cavities was set at 3:1 w/w between GOx (6 mg mL^{-1}) and CAT (2 mg mL^{-1}), a selection based on prior work in our group.[22] Next, the enzymes were crosslinked by the crosslinking agent genipin.[31–33] This method offers the advantages of maintaining the concentration of loaded enzymes and improving enzyme stability within the stomatocyte cavity.[11,22] To gain deeper insight into the spatial distribution of enzymes within the stomatocytes, cryo-TEM was employed, revealing enzyme aggregation within the stomatocytes' cavity (Figures 1d and S5).[32] Subsequently, the total enzyme loading efficiency was determined using the bicinchoninic acid protein assay (BCA) (Figures 1e and S6), which amounted to 23.7%, with a total enzyme concentration of 3.8 mg mL^{-1}, with empty stomatocytes serving as a control group. These findings confirmed the successful formation of c-CLEnM.

Mannosylated Nanomotor Interaction with MBL

After confirming the formation of c-CLEnM, a mannose-functional glycopolymer was conjugated to their surface. As illustrated in Figure 2a, a conjugation process was conducted via CuAAC click chemistry, utilizing azido stomatocytes and alkyne mannose glycopolymer. The alkyne mannose glycopolymer was synthesized via reversible addition-fragmentation chain transfer (RAFT), as detailed in previous studies.[34] Characterization of the resulting products was conducted using ^{1}H NMR spectroscopy and GPC (Figures S7–S13). Prior to conjugation with stomatocytes, a model CuAAC reaction was performed with N_3—PEG_{67}—OH and the alkyne mannose glycopolymer. The clicked product

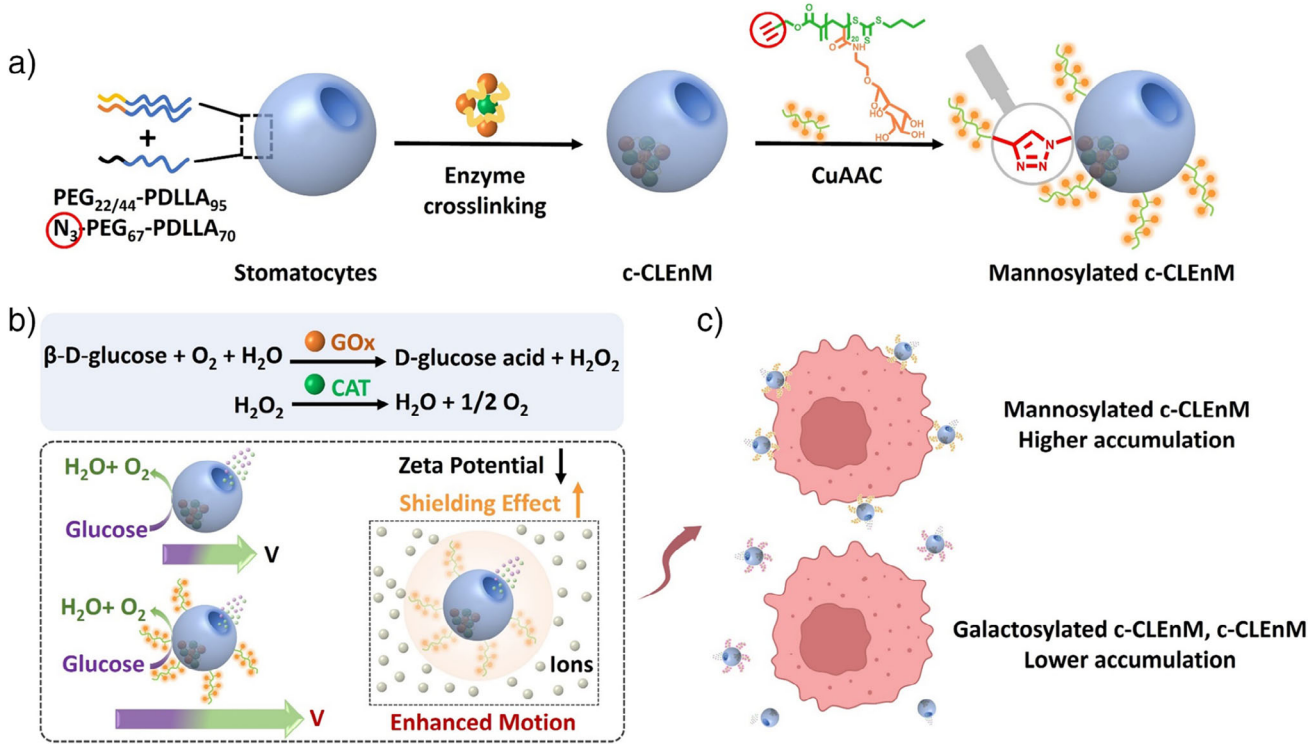

Scheme 1. Schematic illustration of mannosylated compartmentalized cross-linked enzymatic nanomotors (Man-c-CLEnM). a) Poly(ethylene glycol)-*b*-poly(D,L-lactide) (PEG-PDLLA) with two different PEG lengths and functionalized with an azide moiety was co-assembled into stomatocytes, encapsulating catalase (CAT) and glucose oxidase (GOx); the enzymes were subsequently crosslinked in the stomatocyte cavity. Mannose glycopolymer was introduced on the nanoparticle surface via Cu-catalyzed azide-alkyne click chemistry. b) The addition of D-glucose leads to a cascade reaction that produces oxygen, leading to motility. The glycopolymer modified on the nanomotors can increase the zeta potential and potentially generate a shielding effect that mitigates the influence of surrounding ions, thus enhancing motility. c) The mannosylated nanomotors show effective accumulation on the Hep G2 cell membrane compared to galactosylated nanomotors and non-decorated nanomotors. Schematic illustrations of cancer cells were created with BioRender.com.

was characterized via GPC and Fourier-transform infrared spectroscopy (FT-IR). Upon conjugation, a discernible shift toward higher molecular weight was evident in the GPC analysis compared to the starting compounds (Figure S14). Additionally, the disappearance of the azide group was observed in the FT-IR spectra (Figure S15).

We then conjugated azido stomatocytes with alkyne mannose glycopolymer through CuAAC (Figure 2a). To determine the conjugation efficiency, the modified stomatocytes were treated with the fluorescent dye sulfo-cy5-DBCO to determine residual azide groups still left on the stomatocyte surface. Via this approach, an efficiency of 84.8% was determined, with empty stomatocytes serving as a control group (Table S1; Figure S16). The morphology of the stomatocytes was determined both before and after the click reaction with SEM (Figure S17). Following functionalization with the mannose glycopolymer, the surface of the mannosylated stomatocytes appeared to be less smooth compared to the untreated stomatocytes. Furthermore, we investigated the presence of the mannose glycopolymer by determining the binding affinity of the modified stomatocytes to the MBL using SPR analysis.[35]

As shown in Figure 2b,c, different concentrations of both mannosylated stomatocytes and mannosylated c-CLEnM between 6 and 0.25 μM were employed to determine the binding effectiveness through MBL. As expected, both mannosylated stomatocytes and mannosylated c-CLEnM showed a significant binding at all concentrations used, whereas non-decorated stomatocytes and c-CLEnM as a negative control did not show any binding with MBL, which confirms the successful modification of stomatocytes with the glycopolymer (Figure 2d,e). It should be noted that even though strong interaction with MBL was obtained for both mannosylated stomatocytes, the binding did not reach saturation or the equilibrium state within 5 min after the injection of the stomatocytes. This behavior reveals that the binding between mannosylated stomatocytes and MBL is slow, which can be explained by the more compact and globular conformation of the glycopolymer chains on the stomatocytes, which may limit the freedom to adopt an optimal multivalency to reach different binding pockets of the MBL. The kinetic parameters of the mannosylated stomatocytes and mannosylated c-CLEnM were determined, including the association rate constant (k_a), the dissociation rate constant (k_d), the affinity constant (K_A), and the equilibrium dissociation constant (K_D). The kinetic parameters were obtained from fitting the experimental SPR curves with a 1:1 Langmuir binding model (Figure 2f). As the dissociation rate constants ($k_d = 2.47$ and $4.42 \times 10^{-4}\ s^{-1}$) were low for both mannosylated stomatocytes and mannosylated c-CLEnM, it indicates that the mannose

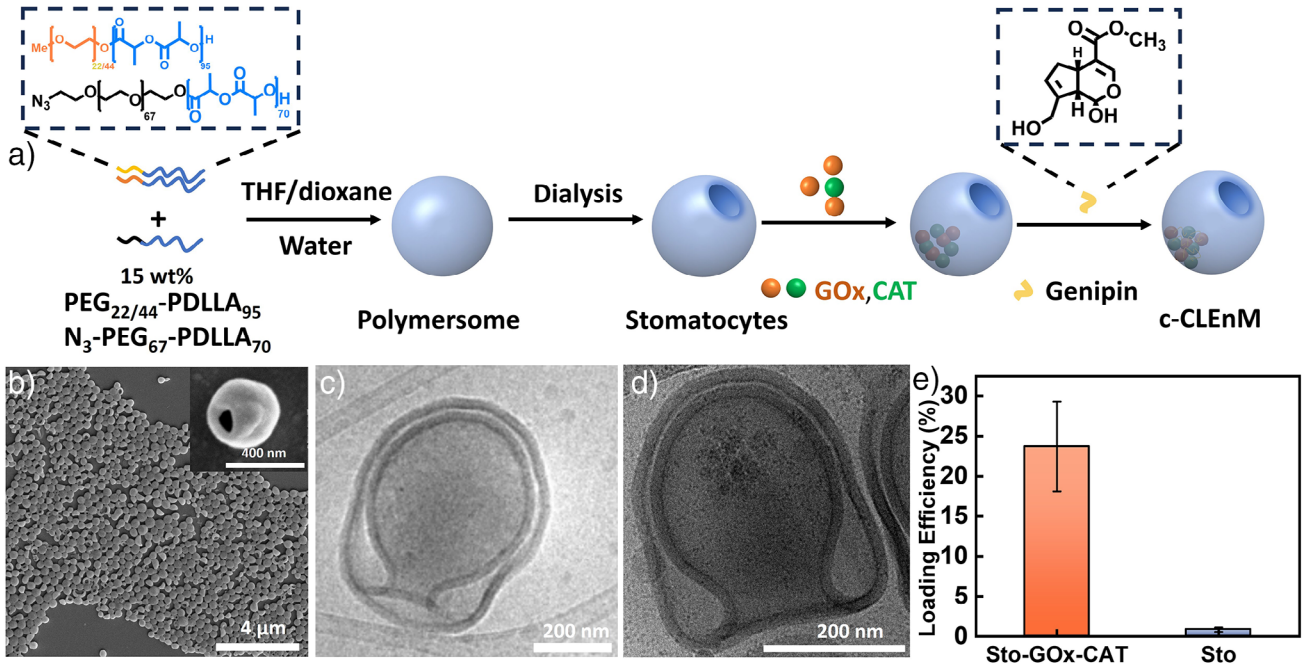

Figure 1. Preparation and characterization of crosslinked enzyme-driven nanomotors (c-CLEnM). a) Schematic illustration of the supramolecular assembly of the c-CLEnM. b) SEM image of empty stomatocytes and zoom in of stomatocytes, scale bar = 4 μm, 400 nm (insert). c) Morphological characterization of empty stomatocytes using cryo-TEM, scale bar = 200 nm. d) Cryo-TEM image revealing the structure of the c-CLEnM, scale bar = 200 nm. e) Quantification of GOx and CAT loading efficiency of enzyme-loaded stomatocytes and empty stomatocytes by using a bicinchoninic acid (BCA) protein assay.

units tend to either remain bound or rebind upon release, rather than dissociate due to the strong interaction between the mannosylated stomatocytes and MBL. In general, both mannosylated stomatocytes and mannosylated c-CLEnM demonstrated a very similar binding profile and strong interactions with MBL, which also shows the minimal and negligible influence of the enzymes in the stomatocyte cavity on the functionalization of the stomatocytes.

Movement Behavior of c-CLEnM, Mannosylated c-CLEnM, and Galactosylated c-CLEnM

To investigate the motility of mannosylated c-CLEnM and c-CLEnM, glucose was added, which served as the driving force for autonomous motion via a cascade reaction. GOx catalyzed the conversion of glucose into hydrogen peroxide and gluconic acid. Subsequently, CAT facilitated the decomposition of hydrogen peroxide into water and oxygen. To explore motility, nanoparticle-tracking analysis (NTA) was employed, involving the tracking of trajectories through individual particle-by-particle analysis of colloidal particles in motion.[22] As shown in Figure 3a,b, the mean square displacement (MSD) and speed of c-CLEnM were directly proportional to the glucose concentration. The average speed of c-CLEnM increased from 6.40 ± 0.38 to 15.53 ± 0.75 μm s^{-1} with increasing glucose concentration, while approximately Brownian motion was detected in the absence of glucose, consistent with previous studies on the motion of c-CLEnM.[22,36,37] The propulsive movement of the nanomotors was determined by fitting the parabolic curve of the MSD dependence on time with the equation $MSD = (4D)\Delta t + (V^2)(\Delta t^2)$.[36] Nanomotors without glucose showed only linear $MSD = (4D)\Delta t$.[36] Additionally, a clear shift in their apparent size, smaller compared to the same structures in the absence of fuel, was observed (Videos S1 and S2; Figure S18); as with NTA, the determination of the nanoparticle diameter is inversely related to the particle's diffusion coefficient.

Subsequently, the motile features of mannosylated c-CLEnM, c-CLEnM, and empty stomatocytes were investigated in MilliQ water with and without glucose. The glucose concentration was maintained at 25 mM, consistent with cell culture conditions (Videos S3 and S4). The MSD (Figure 3c) revealed that both mannosylated c-CLEnM and c-CLEnM exhibited a parabolic trajectory shape in 25 mM glucose solution, indicating ballistic motion at speeds of 13.60 ± 0.46 and 11.80 ± 0.27 μm s^{-1}, respectively. After conjugation with the mannose glycopolymer, mannosylated c-CLEnM exhibited a slightly faster speed than c-CLEnM, while both demonstrated similar overall motility.

Furthermore, to mimic autonomous targeted motion within a cellular environment, the motility of mannosylated c-CLEnM, c-CLEnM, and empty stomatocytes was further evaluated in a cell culture environment by using a live cell imaging solution with and without 25 mM glucose. As shown in Figure 3d; Videos S5 and S6, the mannosylated c-CLEnM and c-CLEnM retained ballistic motion in the presence of 25 mM glucose. Notably, the speed of c-CLEnM decreased significantly to 5.83 ± 0.38 μm s^{-1}

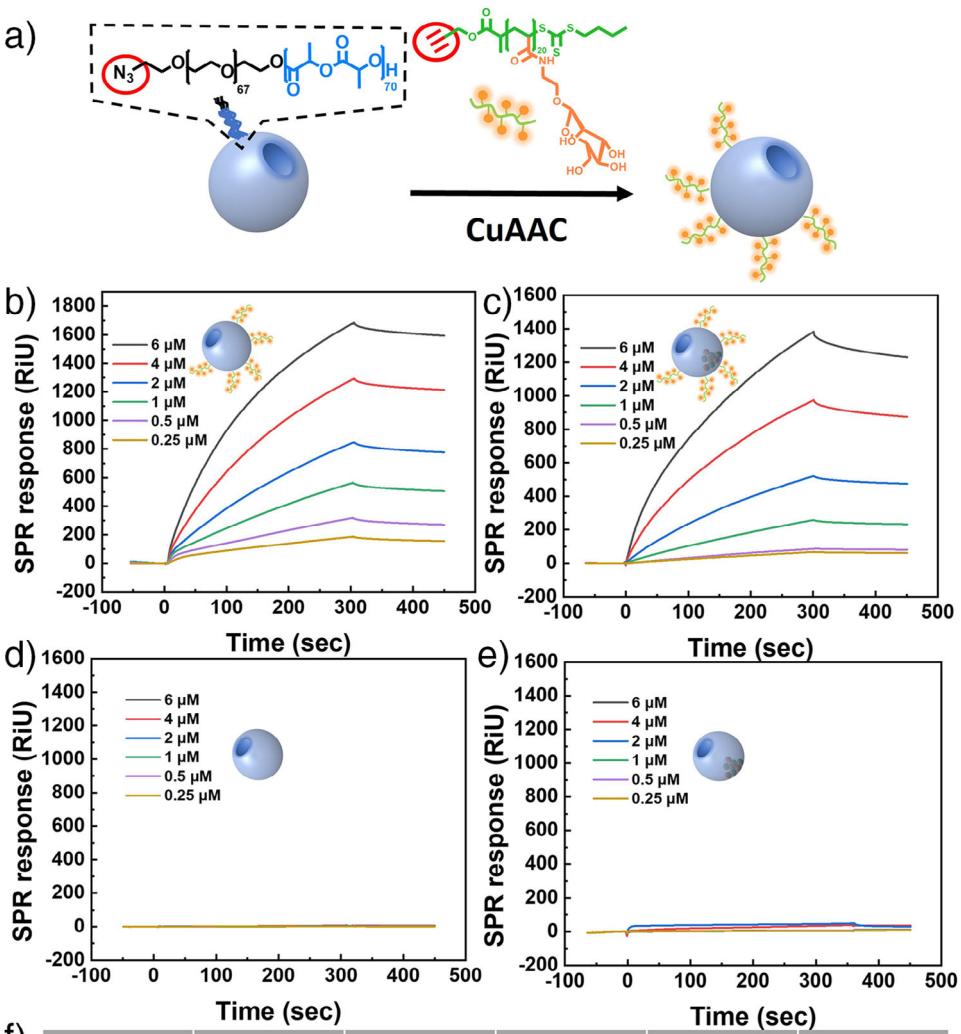

f)

	k_a ($M^{-1}s^{-1}$)	k_d (s^{-1})	R_{max} (RU)	K_A (M^{-1})	K_D (M)
Man-stomatocytes	247	$2.47*10^{-4}$	5960	$1*10^{6}$	$1*10^{-6}$
Man-c-CLEnM	290	$4.42*10^{-4}$	3310	$6.56*10^{5}$	$1.53*10^{-6}$

Figure 2. Characterization of mannosylated stomatocytes. a) Schematic illustration of conjugating mannose glycopolymer to the surface of mannosylated stomatocytes. b) Surface plasmon resonance (SPR) analysis illustrating the binding of mannosylated stomatocytes (Man-stomatocytes) with mannose-binding lectin (MBL). c) SPR analysis demonstrating the binding of mannosylated c-CLEnM (Man-c-CLEnM) with MBL. d) SPR analysis of the binding of empty stomatocytes with MBL. e) SPR analysis of the binding of c-CLEnM with MBL. f) Kinetic values (k_a, k_d, R_{max}, K_A, K_D) obtained from fitting experimental SPR curves with a 1:1 Langmuir binding model.

(Figure 3e). Intriguingly, mannosylated c-CLEnM maintained a speed of 13.47 ± 0.34 μm s^{-1}, comparable to its performance in glucose-containing MilliQ water and representing a remarkable > 2-fold enhancement relative to c-CLEnM. These results highlight the marked effect of glycopolymer modification on enhancing motility in the ionic cell culture environment (Figure 3d,e). In addition, mannosylated c-CLEnM and c-CLEnM in the absence of glucose, as well as empty stomatocytes at both 25 and 0 mM glucose, exhibited typical Brownian motion, with linear MSD fittings (Figure 3c,d). The addition of glucose to empty stomatocytes confirmed that glucose did not affect either Brownian motion or the extracted trajectories, consistent with previous studies.[22,36] To further validate this interesting observation of the universality of glycopolymer-mediated motility enhancement in the cell culture environment, an azido nanomotor was modified with alkyne galactose polymer. The alkyne galactose glycopolymer was also synthesized via the RAFT method, and characterization of the monomer and polymer was conducted using ^{1}H NMR spectroscopy and GPC (Figures S19–S22). Besides, the sizes of galactosylated c-CLEnM, mannosylated c-CLEnM, c-CLEnM, and empty stomatocytes were similar in MilliQ water. After glycopolymer modification, the nanomotor size distribution became more uniform, resulting in improved monodispersity (Figure S23). Their sizes also did not change significantly in ionic

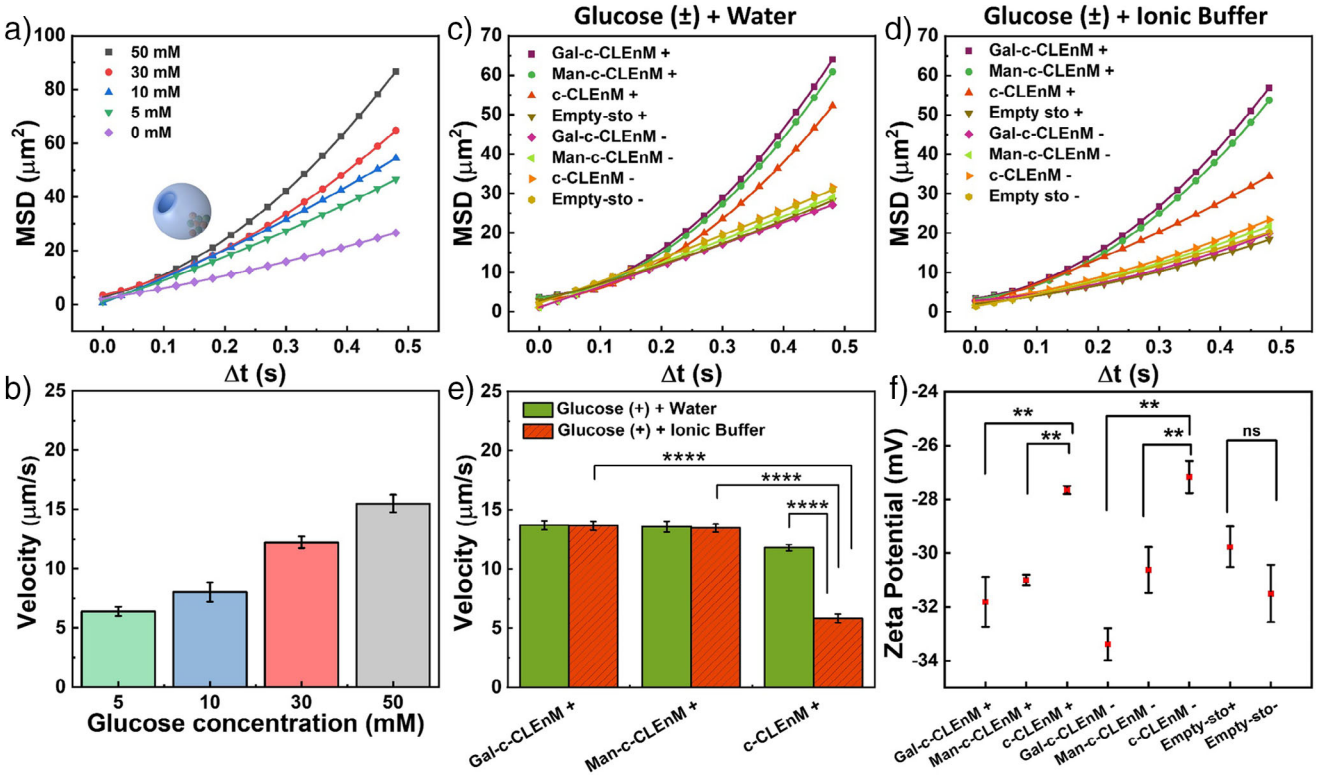

Figure 3. Motion behavior of galactosylated c-CLEnM, mannosylated c-CLEnM, c-CLEnM, and empty stomatocytes. a) MSD curves of c-CLEnM as a function of a range of glucose concentrations (0, 5, 10, 30, 50 mM). b) Average speed of c-CLEnM 6.40 ± 0.38 (5 mM), 8.04 ± 0.80 (10 mM), 12.23 ± 0.50 (30 mM), 15.53 ± 0.75 (50 mM). c) MSDs of galactosylated c-CLEnM, mannosylated c-CLEnM, c-CLEnM, and empty stomatocytes in the presence of glucose (+, 25 mM) and absence of glucose (−) in MilliQ water. d) MSDs of galactosylated c-CLEnM, mannosylated c-CLEnM, c-CLEnM, and empty stomatocytes in the presence (+, 25 mM) and absence of glucose (−) in live cell imaging solution. e) Average speed of galactosylated c-CLEnM, mannosylated c-CLEnM, and c-CLEnM in the presence of glucose (+, 25 mM) in MilliQ water and live cell imaging solution. f) Zeta potential of galactosylated c-CLEnM, mannosylated c-CLEnM, c-CLEnM, and empty stomatocytes in the presence (+, 25 mM) and absence of glucose (−), in live cell imaging solution. $^{**}p < 0.01$; NA, not significant, calculated by *t*-test.

buffer compared to MilliQ water (Figure S24), indicating their good stability under physiological conditions. The motile features of galactosylated c-CLEnM were analyzed under identical conditions (Videos S7 and S8). Regardless of medium, whether glucose-containing MilliQ water or ionic buffer, galactosylated c-CLEnM exhibited sustained ballistic motion with speeds of 13.70 ± 0.38 and 13.66 ± 0.38 μm s^{-1}, respectively. These results confirm that nanomotors modified with glycopolymers display significantly enhanced motility compared to c-CLEnM, underscoring the positive influence of glycopolymer modification on motor performance in an ionic environment.

To gain a better understanding of the mechanism by which glycopolymers enhanced motility, we measured the zeta potential of glycopolymer-modified nanomotors and empty stomatocytes with or without 25 mM glucose (Figure 3f). In glucose-containing ionic buffer, c-CLEnM displayed a less negative zeta potential (−27.65 ± 0.15 mV) compared to empty stomatocytes (−29.76 ± 0.75 mV). This increase may be attributed to enzyme distribution dynamics within stomatocytes, where some enzymes likely attach to the PEG layer on the particle surface. Upon conjugation with glycopolymers, the zeta potential of glycosylated c-CLEnM reverted to nearly its original levels. Specifically, mannosylated c-CLEnM (−31.0 ± 0.20 mV) and galactosylated c-CLEnM (−31.8 ± 0.93 mV) exhibited lower zeta potentials than c-CLEnM (−27.65 ± 0.15 mV) in glucose-containing ionic buffer. A similar trend was observed in the absence of glucose, with mannosylated c-CLEnM (−30.6 ± 0.85 mV) and galactosylated c-CLEnM (−33.4 ± 0.60 mV) displaying lower potentials than c-CLEnM (−27.2 ± 0.60 mV). Furthermore, no significant difference in zeta potential was observed between empty stomatocytes in ionic buffer with or without glucose. These results indicate that glucose does not affect the surface charge of the nanoparticles.

Hence, the improved self-propulsion capabilities of the glycopolymer modified enzyme-powered nanomotors may be attributed to the ionic self-diffusiophoretic mechanism. This mechanism involves electric field generation through ionic gradients, where the effect of external ions on self-propulsion could be explained by a hindrance of the product gradients, thus reducing motion capabilities.[38] Modifying the surface of nanomotors with glycopolymers increases the surface charge, potentially generating a shielding effect that mitigates the influence of surrounding ions. Consequently, this modification improves the ionic tolerance of the nanomotors, ultimately boosting their performance. This mechanism is analogous to

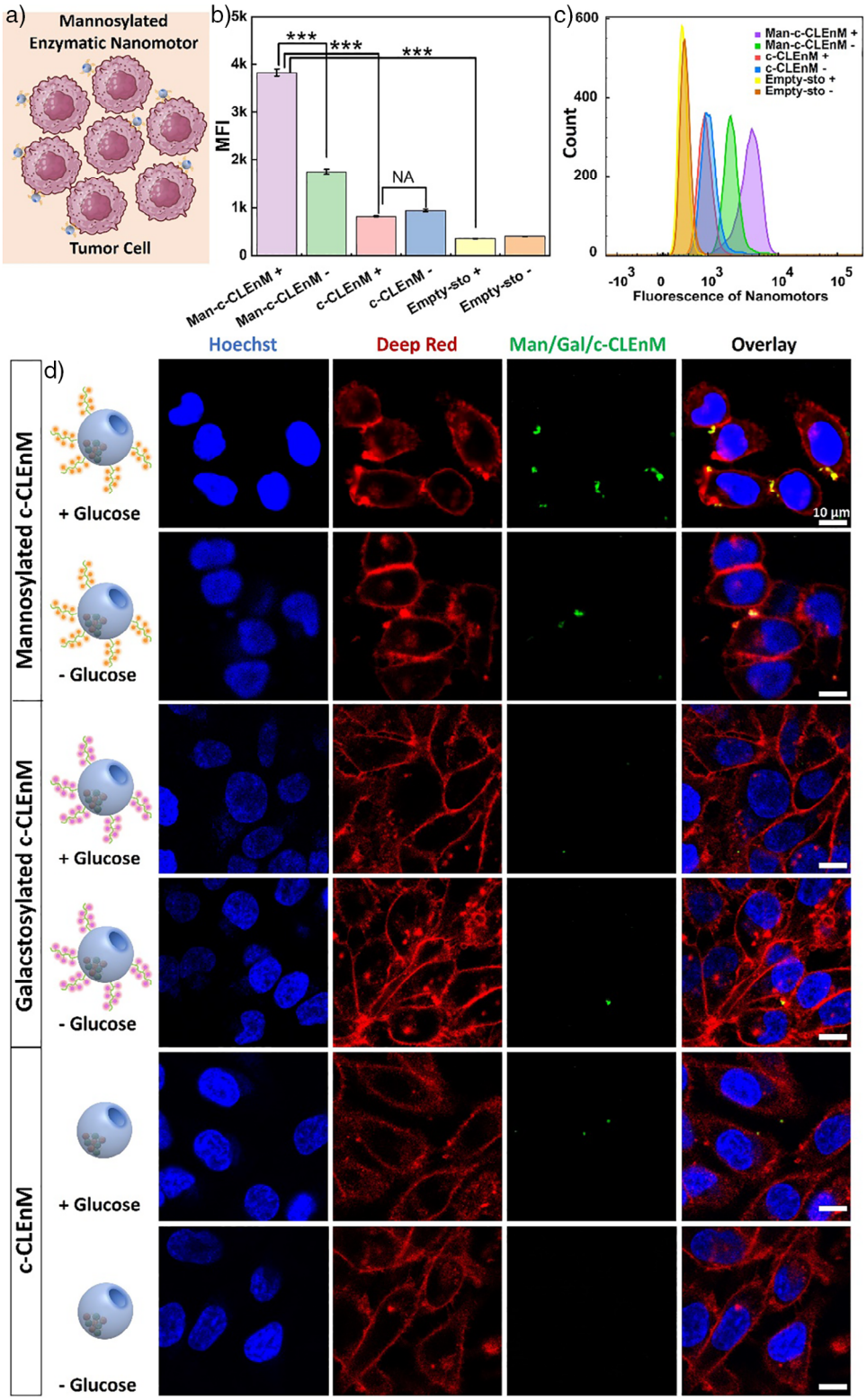

Figure 4. Evaluation of active cell targeting of mannosylated c-CLEnM toward Hep G2 cells. a) Schematic illustration of mannosylated c-CLEnM targeting cancer cells. b) Flow cytometry mean fluorescence intensities of Hep G2 cells treated with representative nanoparticles were measured in the presence (25 mM glucose, DMEM) and absence of glucose ($n = 2$); ***$p < 0.001$; NA, not significant, calculated by *t*-test. c) Flow cytometry histograms of Hep G2 cells treated with mannosylated c-CLEnM, c-CLEnM, and empty stomatocytes in the presence (25 mM glucose, DMEM) and absence of glucose. d) Magnified confocal laser scanning microscopy (CLSM) images of Hep G2 cells incubated with mannosylated c-CLEnM, galactosylated c-CLEnM, and c-CLEnM for 2 h in the presence (25 mM glucose, DMEM) and absence of glucose, scale bar = 10 μm. (+): in the presence of glucose, (−): in the absence of glucose. Schematic illustrations of cancer cells were created with BioRender.com.

that observed in urease micromotors coated with mPEG.[30] Similarly, the increase in negative zeta potential due to mPEG coating suggests higher electrophoretic mobility, raising the possibility that mPEG enhances the electrophoretic effect of ionic self-diffusiophoresis, which also exhibited higher speed in an ionic environment.[30] In addition, only a slight increase in motion was observed in a glucose-containing MilliQ water after glycopolymer modification. This could be attributed to the requirement for a significant ionic gradient around the particles to achieve effective motion.

Active Cell Targeting Based on Receptor-Dependent Binding

Importantly, mannose polymer modification not only alters the surface charge but also introduces targeting properties toward cancer cells, facilitating precise navigation in complex biological environments. Therefore, we examined the effect of glycopolymer modification on cell uptake (Figure 4a). To assess the in vitro cell uptake efficiency of our nanomotors, Hep G2 cells were incubated with mannosylated c-CLEnM and control groups for 2 h, followed by analysis using fluorescence-activated cell sorting (FACS). Here, we cultured the cells in DMEM containing 25 mM glucose. The results (Figure 4b,c) illustrate that cells exposed to mannosylated c-CLEnM in the presence of glucose exhibited more than twice the level of fluorescence compared to cells where fuel was absent. This indicates that autonomous motion using glucose enhances the nanomotor's efficacy in cancer cell uptake. Furthermore, compared to non-mannosylated c-CLEnM at the same glucose concentration, the targeted nanomotors displayed a significantly higher fluorescence. The accumulation on the Hep G2 cells was contributed to the synergistic effect of glycopolymer modification, which led to both a higher motility and targeting ability toward the cancer cells.[39]

To study in more detail the synergy of the mannosylated c-CLEnM regarding their interaction with Hep G2 cells, their cell targeting efficiency was compared with galactosylated c-CLEnM, c-CLEnM, and empty stomatocytes, all labelled with FITC, for a duration of 2 h, both in the presence and absence of glucose. CLSM was employed for this investigation. As depicted in Figures 4d and S25, S26, cells exposed to mannosylated c-CLEnM in the presence of glucose exhibited the highest fluorescence in the same time period, which demonstrated the highest binding efficiency to the cell membrane when DMEM containing 25 mM glucose was present, compared to the control groups. This observation closely aligns with the results obtained from FACS analysis (Figure 4b,c).[26–29] Together with the motor function, this leads to rapid targeting of specific cancer cells, thereby reducing the time required for cell localization. Even though galactosylated nanomotors displayed a similar speed during autonomous motion compared to the mannosylated ones, the Hep G2 cells lack the ability for a strong binding with galactose. To demonstrate that MBLs do not interact with galactose moieties, we conducted SPR with the galactosylated nanomotors and MBL and did not show any binding signals (Figure S27). Next, to further confirm the uptake mechanism of mannosylated nanomotors by Hep G2 cells through the MR, we investigated receptor-mediated endocytosis, which is clathrin-dependent.[40] The cells were pretreated with the clathrin inhibitor chlorpromazine (10 μg mL^{-1}) for 30 min, followed by incubation with mannosylated nanomotors for 2 h in DMEM containing 25 mM glucose. A significantly reduced fluorescence signal of the nanomotors was detected compared to the unpretreated cells, indicating successful inhibition of uptake (Figure S28). These findings support that mannosylated nanomotors are internalized by Hep G2 cells through MR-mediated, clathrin-dependent endocytosis. Additionally, c-CLEnM and empty stomatocytes, whether in the presence or absence of glucose, only showed similar and limited fluorescence.

When the cells were incubated for 6 h with nanomotors and empty stomatocytes, the mannosylated c-CLEnM in the presence of glucose still led to the highest cell fluorescence, indicating greater binding to the cell membrane, with some nanomotors being internalized by the cancer cells (Figures S29–S30).

Conclusion

In summary, mannosylated compartmentalized cross-linked enzymatic nanomotors (c-CLEnM) with elevated autonomous motion were developed for the efficient and specific targeting of Hep G2 cancer cells. We employed biodegradable, bowl-shaped stomatocytes to encapsulate GOx and CAT within their nanocavity, followed by a crosslinking reaction to ensure stable encapsulation, thus supporting the autonomous motion of stomatocytes in the presence of glucose. Additionally, the stomatocytes were functionalized with mannose glycopolymer to achieve specific binding with receptors that are expressed on Hep G2 cells. In glucose-containing cell culture medium, mannosylated c-CLEnM exhibited high and rapid targeting efficiency, attributed to a synergistic effect of the glycopolymer modification. This modification enhanced motor motility by improving the ionic self-diffusiophoretic effect. Additionally, the glycopolymer reduced the surface charge, potentially generating a shielding effect that mitigated the influence of surrounding ions. This increase in speed and active targeting capability led to a significant accumulation of the nanomotors on the Hep G2 cell membrane. Beyond altering surface charge and overcoming the motion limitations imposed by ion tolerance in physiological environments, mannose glycopolymer modification also conferred targeting capabilities toward cancer cells. This study underscores the importance of understanding the effect of nanomotor surface modification, which in this case simultaneously enhanced both targeting efficiency and motility.

Experimental Section

The data that support the findings of this study are available in the Supporting Information of this article.

Acknowledgements

Y.L. and R.T. received funding from the European Union's Horizon 2020 research and innovation program under the Marie Skłodowska-Curie grant agreement no 859416 (BIOMOLMACS). J.H. furthermore acknowledges funding by The Dutch Ministry of Education, Culture and Science, Gravitation Program, grant number 024.005.020, and the Spinoza premium SPI 72–259.

Conflict of Interests

The authors declare no conflict of interest.

Data Availability Statement

The data that support the findings of this study are available from the corresponding author upon reasonable request.

Keywords: Cancer cell targeting · Enhanced autonomous motion · Mannosylated enzymatic nanomotors · Stomatocytes

[1] R. Dreyfus, J. Baudry, M. L. Roper, M. Fermigier, H. A. Stone, J. Bibette, *Nature* **2005**, *437*, 862–865.
[2] S. Palagi, P. Fischer, *Nat. Rev. Mater.* **2018**, *3*, 113–124.
[3] S. Sengupta, M. E. Ibele, A. Sen, *Angew. Chem. Int. Ed.* **2012**, *51*, 8434–8445.
[4] W. Wang, *J. Am. Chem. Soc.* **2023**, *145*, 27185–27197.
[5] Z. Ye, Y. Wang, S. Liu, D. Xu, W. Wang, X. Ma, *J. Am. Chem. Soc.* **2021**, *143*, 15063–15072.
[6] M. Xuan, Z. Wu, J. Shao, L. Dai, T. Si, Q. He, *J. Am. Chem. Soc.* **2016**, *138*, 6492–6497.
[7] Z. Wu, T. Li, W. Gao, T. Xu, B. Jurado-Sánchez, J. Li, W. Gao, Q. He, L. Zhang, J. Wang, *Adv. Funct. Mater.* **2015**, *25*, 3881–3887.
[8] M. Xuan, J. Shao, J. Zhao, Q. Li, L. Dai, J. Li, *Angew. Chem. Int. Ed.* **2018**, *57*, 6049–6053.
[9] Y. Tu, F. Peng, A. Adawy, Y. Men, L. K. Abdelmohsen, D. A. Wilson, *Chem. Rev.* **2016**, *116*, 2023–2078.
[10] Y. Feng, Y. Yuan, J. Wan, C. Yang, X. Hao, Z. Gao, M. Luo, J. Guan, *Appl. Phys. Rev.* **2021**, *8*, 011406.
[11] B. J. Toebes, F. Cao, D. A. Wilson, *Nat. Commun.* **2019**, *10*, 5308.
[12] A. C. Hortelão, T. Patiño, A. Perez-Jiménez, À. Blanco, S. Sánchez, *Adv.Funct. Mater.* **2017**, *28*, 1705086.
[13] X. Ma, A. C. Hortelao, T. Patino, S. Sanchez, *ACS Nano* **2016**, *10*, 9111–9122.
[14] A. C. Hortelao, R. Carrascosa, N. Murillo-Cremaes, T. Patino, S. Sanchez, *ACS Nano* **2019**, *13*, 429–439.
[15] B. Esteban-Fernández de Ávila, A. Martín, F. Soto, M. A. Lopez-Ramirez, S. Campuzano, G. M. Vásquez-Machado, W. Gao, L. Zhang, J. Wang, *ACS Nano* **2015**, *9*, 6756–6764.
[16] T. Zhao, R. Terracciano, J. Becker, A. Monaco, G. Yilmaz, C. R. Becer, *Biomacromolecules* **2022**, *23*, 543–575.
[17] L. Li, R. Zhang, W. Gu, Z. P. Xu, *Nanomedicine* **2018**, *14*, 2355–2364.
[18] M. S. Wadhwa, K. G. Rice, *J. Drug. Target.* **1995**, *3*, 111–127.
[19] G. Yilmaz, C. R. Becer, *Polym. Chem.* **2015**, *6*, 5503–5514.
[20] C. Pifferi, R. Fuentes, A. Fernandez-Tejada, *Nat. Rev. Chem.* **2021**, *5*, 197–216.
[21] Y. Zhang, L. Wu, Z. Li, W. Zhang, F. Luo, Y. Chu, G. Chen, *Biomacromolecules* **2018**, *19*, 2098–2108.
[22] L. K. Abdelmohsen, M. Nijemeisland, G. M. Pawar, G. J. Janssen, R. J. Nolte, J. C. van Hest, D. A. Wilson, *ACS Nano* **2016**, *10*, 2652–2660.
[23] L. K. E. A. Abdelmohsen, D. S. Williams, J. Pille, S. G. Ozel, R. S. M. Rikken, D. A. Wilson, J. C. M. van Hest, *J. Am. Chem. Soc.* **2016**, *138*, 9353–9356.
[24] I. A. B. Pijpers, L. K. E. A. Abdelmohsen, D. S. Williams, J. C. M. van Hest, *ACS Macro Lett.* **2017**, *6*, 1217–1222.
[25] C. Zhou, C. Gao, Y. Wu, T. Si, M. Yang, Q. He, *Angew. Chem. Int. Ed.* **2022**, *61*, e202116013.
[26] W. Fan, X. Yang, F. Huang, X. Tong, L. Zhu, S. Wang, *Oncol. Lett.* **2019**, *18*, 3218–3226.
[27] X. Gai, K. Tu, Z. Lu, X. Zheng, *Int. J. Mol. Sci.* **2014**, *15*, 15011–15025.
[28] C. Guan, Y. Zhao, Y. Hou, G. Shan, D. Yan, Y. Liu, *Talanta* **2018**, *182*, 314–323.
[29] M. Kim, M. Jeong, S. Hur, Y. Cho, J. Park, H. Jung, Y. Seo, H. A. Woo, K. T. Nam, K. Lee, H. Lee, *Sci. Adv.* **2021**, *7*, eabf4398.
[30] X. Arque, X. Andres, R. Mestre, B. Ciraulo, J. Ortega Arroyo, R. Quidant, T. Patino, S. Sanchez, *Research.* **2020**, *2020*, 2424972.
[31] M. T. De Martino, F. Tonin, N. A. Yewdall, M. Abdelghani, D. S. Williams, U. Hanefeld, F. P. J. T. Rutjes, L. K. E. A. Abdelmohsen, J. C. M. van Hest, *Chem. Sci.* **2020**, *11*, 2765–2769.
[32] V. G. Tacias-Pascacio, E. García-Parra, G. Vela-Gutiérrez, J. J. Virgen-Ortiz, Á. Berenguer-Murcia, A. R. Alcántara, R. Fernandez-Lafuente, *Catalysts* **2019**, *9*, 1035.
[33] S. Velasco-Lozano, F. López-Gallego, J. C. Mateos-Díaz, E. Favela-Torres, *Biocatal* **2016**, *1*, 166–177.
[34] S. Perrier, *Macromol.* **2017**, *50*, 7433–7447.
[35] C. R. Becer, *Macromol. Rapid Commun.* **2012**, *33*, 742–752.
[36] H. Che, J. Zhu, S. Song, A. F. Mason, S. Cao, I. A. B. Pijpers, L. Abdelmohsen, J. C. M. van Hest, *Angew. Chem. Int. Ed.* **2019**, *58*, 13113–13118.
[37] J. Shao, S. Cao, H. Wu, L. K. E. A. Abdelmohsen, J. C. M. van Hest, *Pharmaceutics* **2021**, *13*, 1833.
[38] J. Wang, Z. Xiong, J. Zheng, X. Zhan, J. Tang, *Acc. Chem. Res.* **2018**, *51*, 1957–1965.
[39] L. Su, R. Li, S. Khan, R. Clanton, F. Zhang, Y. N. Lin, Y. Song, H. Wang, J. Fan, S. Hernandez, A. S. Butters, G. Akabani, R. MacLoughlin, J. Smolen, K. L. Wooley, *J. Am. Chem. Soc.* **2018**, *140*, 1438–1446.
[40] L. Martinez-Pomares, *J. Leukoc. Biol.* **2012**, *92*, 1177–1186.

Manuscript received: March 11, 2025
Revised manuscript received: March 28, 2025
Accepted manuscript online: April 01, 2025
Version of record online: April 10, 2025